AGU PUBLICATIONS

Geophysical Research Letters

RESEARCH LETTER
10.1002/2015GL065868

Key Points:
- Precise scaling using Green's functions improves time reverse imaging of tsunami source
- Substantially improved, near-real-time source estimates when precomputed Green's functions exist
- Excellent ability to predict far-field waveforms for tsunami early warning in real time

Supporting Information:
- Text S1 and Figures S1–S9
- Readme

Correspondence to:
M. J. Hossen,
jakir.hossen@anu.edu.au

Citation:
Hossen, M. J., P. R. Cummins, J. Dettmer, and T. Baba (2015), Time reverse imaging for far-field tsunami forecasting: 2011 Tohoku earthquake case study, *Geophys. Res. Lett.*, *42*, 9906–9915, doi:10.1002/2015GL065868.

Received 21 AUG 2015
Accepted 22 OCT 2015
Accepted article online 4 NOV 2015
Published online 22 NOV 2015

Time reverse imaging for far-field tsunami forecasting: 2011 Tohoku earthquake case study

M. Jakir Hossen[1], Phil R. Cummins[1], Jan Dettmer[1], and Toshitaka Baba[2]

[1]Research School of Earth Sciences, Australian National University, Canberra, ACT, Australia, [2]Institute of Technology and Science, University of Tokushima, Tokushima, Japan

Abstract This paper describes a new method for forecasting far-field tsunamis by combining aspects of least squares tsunami source inversion (LSQ) with time reverse imaging (TRI). This method has the same source representation as LSQ but uses TRI to estimate initial sea surface displacement. We apply this method to the 2011 Japan tsunami, and the results show that the method produces tsunami waveforms of excellent agreement with observed waveforms at both near- and far-field stations not used in the source estimation. The spatial distribution of cumulative sea surface displacement agrees well with other models obtained in more sophisticated inversions, but resolve source kinematics are not well resolved. The method has potential for application in tsunami warning systems, as it is computationally efficient and can be used to estimate the initial source model by applying precomputed Green's functions in order to provide more accurate and realistic tsunami predictions.

1. Introduction

The 2011 Tohoku-oki earthquake triggered one of the world's most destructive tsunamis, in which near-field impacts included > 18,000 fatalities and $220 billion in economic loss [*National Geophysical Data Center/World Data Service*, 2015]. However, the impact of this massive tsunami was not limited to the near field. In the far field along U.S. Pacific coast, virtually every port and maritime facility along U.S. West Coast was adversely affected by surges and currents, with over $20 million in damage caused to the port at Crescent City alone [*Wilson et al.*, 2013]. The tsunami also caused considerable far-field damage along the coast of New Zealand [*Borrero et al.*, 2013]. Major far-field impacts have also been caused by earlier tsunami events, with the 2004 Indian Ocean tsunami resulting in 60,000 deaths at distances thousands of kilometers from the tsunami source [*Inderfurth et al.*, 2005].

Because of the potential for destructive far-field impacts from large tsunamis, considerable effort has been devoted to rapid, far-field tsunami forecasting. The U.S. National Oceanic and Atmospheric Administration (NOAA) has implemented a rapid tsunami forecast program called Short-term Inundation Forecast for Tsunamis [*Gica et al.*, 2008; *Percival et al.*, 2011] since 2008, which uses earthquake and sea level data to rapidly forecast waveforms for trans-Pacific tsunamis. NOAA has also implemented the Alaska Tsunami Forecast Model [*Kowalik et al.*, 2005] and the real-time tsunami forecast model (RIFT) [*Wang et al.*, 2012]. More recently, the French Polynesian tsunami warning center has developed a new tsunami forecast tool, named MERIT, for tsunami warning based on tsunami propagation numerical model [*Jamelot and Reymond*, 2015]. And *Maeda et al.* [2015] have implemented a data assimilation (DA) technique in tsunami forecasting that does not rely on earthquake source parameters. Many tsunami warning centers that provide tsunami warnings in the Indian Ocean operate similar forecasting systems [*Greenslade et al.*, 2014]. All of these forecasting systems rely on earthquake source parameters to initialize forecasts, and some use observations of sea level data to calibrate the initial forecast.

Except for RIFT, MERIT, and DA, all current forecast systems rely on precomputed databases of tsunamis for suites of either scenario earthquakes or basis earthquakes, typically subduction megathrust earthquakes, from which an appropriate selection or combination is used to forecast the tsunami for an actual earthquake. As noted by *Wang et al.* [2012], database forecast systems suffer from the fundamental limitation that they cannot accurately forecast tsunamis generated by earthquakes that are not well represented in the database, typically outer rise events or large, submarine strike-slip events such as occurred in 2012 off northwest Sumatra. The parameterization of an event database also limits the ability to forecast an actual event,

with *Greenslade et al.* [2014] noting that the variation among forecasts of Indian Ocean tsunami warning systems has, on average, a standard deviation of the maximum amplitudes that is approximately 62% of its mean value.

Even a real-time forecasting system may have limited ability to accurately forecast tsunamis if it assumes the tsunami source is well represented by earthquake parameters alone. The moment tensor of an earthquake used for fault orientation and seismic moment inevitably has estimation error; scaling relationships such as *Wells and Coppersmith* [1994] used to set fault parameters such as length and width have considerable scatter, and large earthquakes often have heterogeneous slip patterns that will result in tsunami excitation different from that predicted by a uniform-slip model. Further approximations are involved in the elastic dislocation modeling of seafloor deformation [*Cummins et al.*, 1998] and the translation of the seafloor deformation to the sea surface displacement that generates the tsunami [*Saito and Furumura*, 2009]. Finally, any forecast method that assumes exclusively earthquake excitation will not produce accurate forecasts when there is a significant nonseismic component to the source as may be the case for the 2011 Tohoku tsunami [*Tappin et al.*, 2008]. These limitations may be less critical if the forecast is calibrated with observed sea level data, but if this includes inversion of tsunami waveforms, it typically involves subjective choices of station weights and regularization parameters that may have significant impact on the source estimate [*Percival et al.*, 2011].

As noted by *Tang et al.* [2012], for accurate forecasting of tsunami impacts it may be desirable to avoid dependence on earthquake source parameters and instead focus on the characteristics of tsunamis themselves. We therefore seek a method based on time reverse imaging for rapid, accurate forecasting of far-field tsunamis that is, to the greatest extent possible, dependent on sea level data alone. Time reverse imaging involves numerically "retransmitting" discrete approximations of time-reversed observed waveforms starting at the point of observation, which results in refocusing at the original source. Early work by *Larmat et al.* [2006, 2008] showed that seismic waves can be successfully refocused in the earthquake source region at a global scale, providing efficient of imaging sources of seismic energy. *Kawakatsu and Montagner* [2008] examined the relationship between inversion and the time reversal method and applied time reversal to moment tensor estimation. More recently, *Bazargani and Snieder* [2013] study how time reversal can be considered an optimization problem to estimate unknown seismic sources in known acoustic and elastic media. *Hossen et al.* [2015a], expanding on a concept first proposed by *Korolev* [2011], developed a time reverse imaging (TRI) method to estimate tsunami source models. In addition to the assumptions of linearity and zero energy loss, which are approximately satisfied only for deep ocean tsunami propagation, a limitation of the method proposed in *Hossen et al.* [2015a] is that amplitude estimation requires a scaling factor which does not take into account effects such as variable bathymetry.

In this paper, we extend the TRI technique by using Green's functions (GFs) which we henceforth refer to as "Green's function-based time reverse imaging" (GFTRI), to achieve more rigorous scaling of the refocused image that takes into account variable bathymetry in the source region. Importantly, since the sea surface displacement is directly inferred, no assumptions about earthquake parameters are made. Further, since no regularization is required, the difficulty of selecting regularization/smoothing parameters is completely avoided. These advantages result in practical simplicity, computational efficiency, and applicability even for complex events that may include contributions from various source components (e.g., seafloor deformation and submarine mass failures). We apply this new approach to the 2011 Tohoku tsunami to estimate the initial sea surface displacement. This approach is computationally efficient and has potential for use in real-time, far-field tsunami warning. We demonstrate its ability to accurately forecast far-field tsunamis by refocusing near-field recordings of the 2011 Tohoku tsunami and using the estimated source to predict the far-field waveforms for this event.

2. Theory

We extend the work of *Hossen et al.* [2015a] on TRI of the tsunami source, by taking into account the effect of varying bathymetry in the source region on the refocused tsunami to substantially improve the source estimate. Let $a_i(t)$ be the amplitude of an incremental variation in sea level having a delta-function-like spatial distribution centered at one of a discrete set of locations $\mathbf{s}_i$, $i = 0, 1, \ldots, n$ and defined over $t \in (0, T)$. $G_i(\mathbf{x}_j, t) = G(\mathbf{x}_j, t; \mathbf{s}_i, 0)$ is the computed GF describing sea level variation at the observation point $\mathbf{x}_j$ due to a point source at $\mathbf{s}_i$, having time dependence $\delta(t)$, where $j = 0, 1, 2, \ldots, p$ is an index over multiple

observation points. Following *Kawakatsu and Montagner* [2008], we denote the time-reversed wavefield at $\mathbf{s}_i$ obtained from a recorded sea level observation $d_j(t)$ at position $\mathbf{x}_j$ as

$$\begin{aligned} \mathrm{TR}_j(\mathbf{s}_i, t) &= G_j(\mathbf{s}_i, t) * d_j(T - t) \\ &= G_i(\mathbf{x}_j, t) * d_j(T - t), \end{aligned} \tag{1}$$

where $*$ denotes convolution and we have used the spatial reciprocity established by *Hossen et al.* [2015a] (see also Figure S1 in the supporting information for the case that includes dispersive effects): $G_i(\mathbf{x}_j, t; \mathbf{s}_i, 0) = G_j(\mathbf{s}_i, t; \mathbf{x}_j, 0)$. That is to say, $\mathrm{TR}_j(\mathbf{s}_i, t)$ is the sea level variation at $\mathbf{s}_i$ that would occur due to a point source at $\mathbf{x}_j$ having time dependence $d_j(T - t)$. In the frequency domain this becomes

$$\mathrm{TR}_j(\mathbf{s}_i, \omega) = e^{i\omega T}[G^*(\mathbf{x}_j, \omega; \mathbf{s}_i, 0) d_j(\omega)]^* , \tag{2}$$

where superscript * denotes the complex conjugate. In *Hossen et al.* [2015a], a TRI reconstruction of the tsunami source for the 2011 Tohoku-oki earthquake was obtained as a linear combination of time-reversed wavefields

$$a_i^{\mathrm{TR}}(t) = \frac{1}{p} \sum_{j=1}^{p} \alpha_{ij} \mathrm{TR}_j(\mathbf{s}_i, T - t). \tag{3}$$

($a_i^{\mathrm{TR}}(t)$ is the TRI estimate for the true sea surface displacement $a_i(t)$.) *Hossen et al.* [2015a] investigated two choices for the scaling factor α_{ij}. For the first choice, the scaling was a constant independent of source position $\mathbf{s}_i$ and observation point $\mathbf{x}_j$. The value for this scaling was chosen to match the extremal values in the observed tsunami waveforms. For the second choice, the scaling depended only on observation point $\mathbf{x}_j$, whose value was chosen so that a tsunami generated by a point source at the earthquake epicenter would preserve its height when reverse-time propagated from $\mathbf{x}_j$. In both cases, the TRI results captured some main features of the tsunami source (peak amplitude and location of peak) but lacked the detailed resolution provided by inversion. In addition, the gross characteristics (e.g., arrival time and amplitude) of the tsunami waveforms predicted by the TRI source models matched those of the observed waveforms reasonably well but did not match detailed features and showed some mismatched amplitudes [see *Hossen et al.*, 2015a].

More rigorously, the scaling parameter α_{ij} can be motivated by the analogy between source imaging and inversion discussed by *Kawakatsu and Montagner* [2008]. The predicted waveforms $\psi(\mathbf{x}_j, t)$ at $\mathbf{x}_j$ due to initial source $a_i(t)$ are given by

$$\psi(\mathbf{x}_j, t) = \sum_{i=0}^{n} G_i(\mathbf{x}_j, t) * a_i(t), \quad j = 0, 1, \ldots, p. \tag{4}$$

Let the frequency domain misfit function, defined to minimize the difference between predicted and observed waveforms at position $\mathbf{x}_j$, be

$$\begin{aligned} J(\omega) &= |\psi(\mathbf{x}_j, \omega) - d_j(\omega)|^2 \\ &= \left| \sum_{i=0}^{n} G_i(\mathbf{x}_j, \omega) a_i(\omega) - d_j(\omega) \right|^2 , \end{aligned} \tag{5}$$

where $d_j(\omega)$ is the Fourier transform of the waveform recorded at $\mathbf{x}_j$. To minimize $J(\omega)$, for any frequency ω, we set $\frac{\partial J}{\partial \hat{a}_i} = 0$, which gives (see the derivation in the supporting information)

$$\sum_{i=0}^{n} G_{i'}^*(\mathbf{x}_j, \omega) G_i(\mathbf{x_j}, \omega) \hat{a}_{ij}(\omega) = G_{i'}^*(\mathbf{x}_j, \omega) d_j(\omega), \tag{6}$$

where i' and i are indices for source location and $\hat{a}_{ij}(\omega)$ denotes the estimate of $a_i(\omega)$ that minimizes the misfit with respect to observation $d_j(\omega)$. The term $G_{i'}^*(\mathbf{x}_j, \omega) G_i(\mathbf{x}_j, \omega)$ can be recognized as the Fourier transform of the cross correlation between the Green's functions for waveforms recorded at $\mathbf{x}_j$ due to point sources at $\mathbf{s}_{i'}$ and $\mathbf{s}_i$. If the $\mathbf{s}_{i'}$ and $\mathbf{s}_i$ are sufficiently separated in space such that tsunami arrivals at $\mathbf{x}_j$ are separated in time, then we can approximate this cross correlation as

$$\int G_{i'}(\mathbf{x}_j, \tau) G_i(\mathbf{x}_j, t + \tau) \mathrm{d}\tau \approx |G_{ij}|^2 \delta_{ii'}, \tag{7}$$

where $\delta_{i'i}$ is the Kronecker delta (one when $i = i'$ and zero otherwise), and $|G_{ij}|^2$ is the autocorrelation of $G_i(\mathbf{x}_j, t)$ at zero lag: $|G_{ij}|^2 = \int |G_i(\mathbf{x}_j, \tau)|^2 \mathrm{d}\tau$. Due to the presence of $\delta_{i'i}$, the sum in equation (6) vanishes, which gives

$$\hat{a}_{ij}(\omega) = \frac{1}{|G_{ij}|^2} G_i^*(\mathbf{x}_j, \omega) d_j(\omega) = \frac{e^{i\omega T}}{|G_{ij}|^2} \mathrm{TR}_j^*(\mathbf{s}_i, \omega). \tag{8}$$

Finally, by averaging the time-reversed wavefields from the p observation points and transforming to the time domain, we can write the GFTRI estimate for the tsunami source as

$$a_i^{\mathrm{TR}}(t) = \frac{1}{p} \sum_{j=1}^{p} \frac{1}{|G_{ij}|^2} \mathrm{TR}_j(\mathbf{s}_i, T - t - \delta t_i). \tag{9}$$

This is equivalent to replacing α_{ij} with $1/|G_{ij}|^2$ in equation (3), and we expect $1/|G_{ij}|^2$ to be a better choice of scaling factor than those considered in *Hossen et al.* [2015a] because it considers the effect of varying bathymetry within the source region on the source estimate. δt_i is a time adjustment that depends on the position and shape of the basis function used in the GF calculation and will be discussed in the next section. Note that time dependence of the source, for times $t > 0$ is recovered simply by reducing the duration of the time-reversed wavefield. Therefore, accounting for kinematic source effects is in principle straightforward. In this new approach, we first select the source area, divide it into a number of source grid points, compute GFs from each grid point with an initial unit amplitude source, reverse the observed waveforms, and convolve them with computed GFs to estimate the amplitude of each initial source. Since the observation points and any tsunami source area of concern are typically known in advance, the Green's functions can be precomputed. In that case, equation (9) does not required any numerical simulation to be performed in real time, nor does it involve matrix inversion or determination of regularization parameters. In this sense it is simpler and more computationally efficient than source inversion and/or real time simulation.

3. Methodology

We compute approximations to the point source GFs, $G_i(\mathbf{x}_j, t)$, described above by solving the linear shallow water wave equations using an initial sea surface height localized near each source grid point $\mathbf{s_i}$. The total number of source grid points is 144, obtained by subdividing the source area (240×540 km) at 30 km intervals. The initial sea surface displacement centered on the source grid point $\mathbf{s_i}$ is given by

$$\eta_i = 0.25 \times [1 + \cos(\pi x_i / L)] \times [1 + \cos(\pi y_i / L)] \,, \quad -L \le x_i, y_i \le L \,, \tag{10}$$

where x_i, y_i measure distance along the Earth's surface in the directions parallel and perpendicular to the trench axis, respectively, the point $x_i = 0$, $y_i = 0$ corresponds to $\mathbf{s_i}$, and we have chosen $L = 30$ km. Note that this basis function has much more compact (and finite) support than the Gaussian basis functions that are typically used in inversions of tsunami waveform data for initial sea surface displacement [e.g., *Hossen et al.*, 2015b; *Saito et al.*, 2011].

The fact that the basis function in equation (10) has finite support means that the sea surface disturbance, instead of starting at $\mathbf{s_i}$ as we have previously assumed, is actually already advanced by a distance $L/2$ when the calculation starts, and this shift needs to be factored in twice to account for the time-reversed propagation. For this reason, as indicated in equation (9), we shift the time-reversed waveform by the factor $\delta t_i = L/\sqrt{gD(\mathbf{s_i})}$ where $D(\mathbf{s_i})$ is the water depth at source grid point i. We found that this correction significantly improves refocused images.

In order to calculate the $G_i(\mathbf{x}_j, t)$, we use the sea surface displacement given by equation (10) as initial condition for the linear shallow water wave equation solver implemented by the program JAGURS [*Baba et al.*, 2014]. JAGURS solves the shallow water equations in spherical coordinates with a linear dispersion term, by implementing a staggered, leapfrog finite difference scheme. In order to cover the stations used in source refocusing (Figure 1), we consider a computational domain extending from 140.0°E–158.0°E and 27.0°N–46.0°N. For this computational domain, bathymetry data are given by combining the GEBCO_08 30″ grid data over the whole domain with the more accurate M7000 map series provided by Marine Information Research Center, Japan Hydrographic Association near Japan. Total simulation time is 9000 s with a time step of $\Delta t = 1$ s so that the stability condition $\Delta t < \Delta x/\sqrt{2gh_{\max}}$ is satisfied [*Baba et al.*, 2014], where $\Delta x = 900$ m and $h_{\max}$ is the maximum still water depth in the computational domain. We use a single grid—i.e., no nesting.

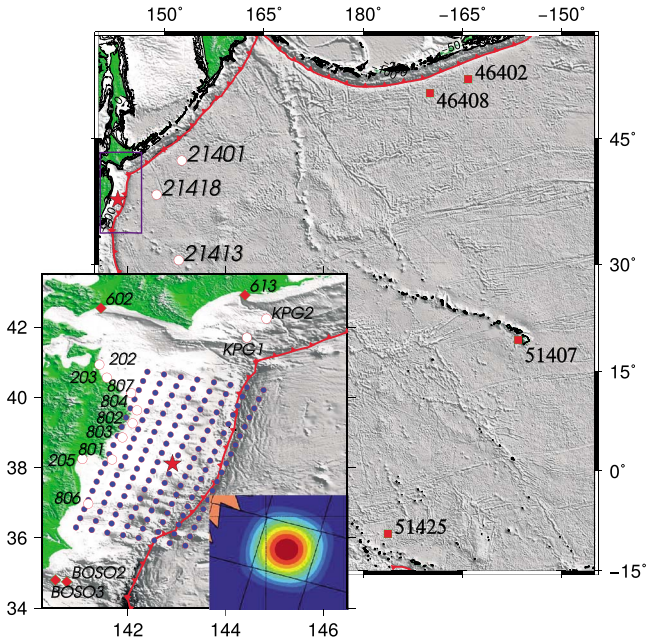

Figure 1. The northern Pacific region considered in this study. Locations where tsunami waveforms were recorded due to the 2011 Japan tsunami are marked: white circles indicate the observations used for tsunami source estimation. The other locations (red squares and diamonds) indicate the observations where waveforms are predicted for comparison (red squares = far field, red diamonds = near field). Red star indicates the earthquake epicenter, and blue dots indicate positions of the $L = 30$ km nodes used in the source estimation. An example of a cosine-tapered basis function (see equation (10)) used for GF computation over a 30×30 km region surrounding each source grid point is given in the inset. The northeast Japan subduction zone trench axis is indicated by the red "sawtooth" curve.

4. Observations

The observed tsunami waveforms generated by the 2011 Tohoku earthquake used in this study were recorded by observation systems operated by several different agencies [e.g., *Tang et al.*, 2012; *Tsushima et al.*, 2009; *Wei et al.*, 2013]. The Deep-ocean Assessment and Reporting of Tsunamis (DART) buoy system is operated by the National Oceanic and Atmospheric Administration (NOAA) [*Titov et al.*, 2005], real-time kinematic Global Positioning System (GPS) buoys by the Nationwide Ocean Wave Information Network for Ports and Harbours, KPG1 and KPG2 by the Japan Agency for Marine-Earth Science and Technology (JAMSTEC) [*Hirata et al.*, 2002], and BOSO2 and BOSO3 by the Japan Meteorological Agency (JMA). The recordings are the most extensive and high quality ever recorded for a megathrust earthquake like the Tohoku-oki event. The locations of observations are given in Figure 1.

5. Results

We apply the new GFTRI approach to estimate a source model for the 2011 Japan tsunami using observed waveforms. In order to image detailed sea surface displacement, we computed Green's functions using the basis functions described in equation (10) as initial condition for sea surface displacement. We use 14 observations (3 DART buoys, 2 OBPGs, 6 GPS buoys, and 3 tide gauges) located around the source region, as indicated in Figure 1. To ensure that the reciprocity principle applies, we choose a minimum distance between the source grid and observation points that is longer than one wavelength. Hence, we consider observations which are located a minimum distance of 90 km from the nearest source grid point.

Images of the refocused source $a_i^{\mathrm{TR}}(t)$ (equation (9)) are displayed in Figure S2 for $t = -240, -120, -60, 0, 60$, and 240 s. Ideally, $a_i^{\mathrm{TR}}(t)$ would be zero for $t < 0$, which corresponds to times prior to the earthquake. At the earthquake origin time $t = 0$, $a_i^{\mathrm{TR}}(t)$ would be nonzero only near the epicenter, and for subsequent times, this disturbance would grow and spread outward over the source area. This would reflect the source kinematics in which fault rupture spreads from the hypocenter over the fault at a rupture velocity of $\sim 1-2$ km/s [*Satake et al.*, 2013]. Clearly, the temporal resolution of the GFTRI method is insufficient to image the time evolution of

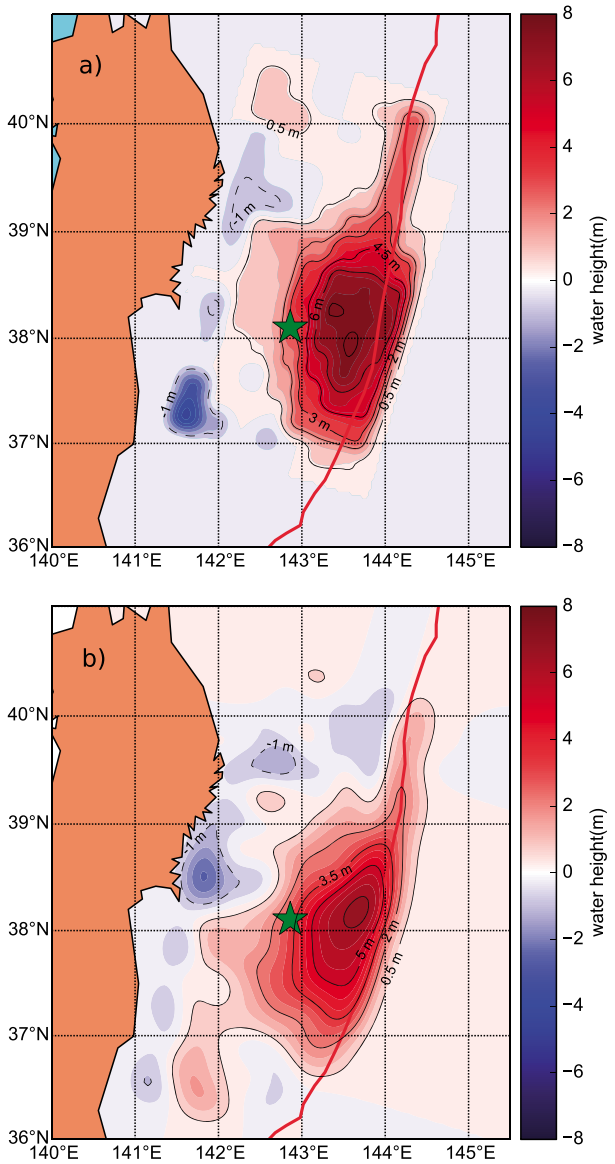

Figure 2. Tsunami source model derived by (top) using Green's function-based time reverse imaging and inferred by (bottom) using conventional source inversion method with source kinematics and dispersion [*Hossen et al.*, 2015b].

the tsunami source, so instead, we see a low-amplitude sea surface displacement that is already spread over the source area at time $t = -240$ s (before the earthquake) and that grows until it reaches a maximum around $t = 0$ to 60 s and begins to diminish thereafter. However, the overall pattern of sea surface displacement is very similar to the cumulative source model (Figure 2b) obtained by *Hossen et al.* [2015b] through an inversion that accounted for source kinematics and dispersive tsunami propagation. It is noteworthy that the $t = 0$ model includes a narrow zone of 1–2 m slip near the subduction zone trench axis between 39 and 40°N, which appears in tsunami-derived source models such as that of *Satake et al.* [2013], but not in models derived from seismic data such as *Yue and Lay* [2011] and *Ammon et al.* [2011]. *Tappin et al.* [2014] suggest that a submarine mass failure occurred at this location, which could result in nonseismic tsunami excitation.

Figure 3 displays the 14 near-field tsunami waveforms that were used to obtain the source estimate in Figure 2a. The observed waveforms are compared to predictions computed using the GFTRI source (Figure 2a) as well as those calculated from the inversion result of *Hossen et al.* [2015b] (Figure 2b). As might be expected, the waveforms calculated using the inversion result of *Hossen et al.* [2015b] provide a better fit to the data,

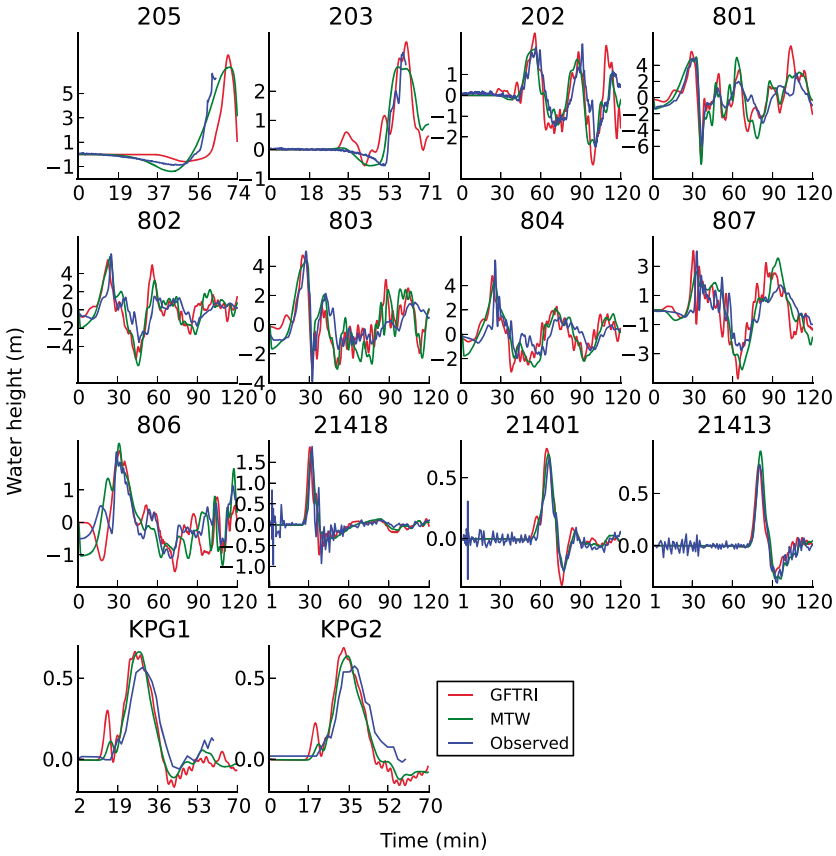

Figure 3. Comparison of observed near-field tsunami waveforms that were used to estimate the GFTRI source, Figure 2a. Observed (blue) waveforms are compared with those calculated using the GFTRI source model (red) and the inversion result of *Hossen et al.* [2015b], Figure 2b (green).

since those were calculated using a source model derived by optimizing the fit to the waveforms. The waveforms calculated from the GFTRI source result, while providing a poorer agreement with the data than those calculated from the inversion result, nevertheless match the amplitudes and dominant periods of the observed waveforms well. We believe that the agreement of waveforms predicted using the GFTRI result with the observed waveforms in Figure 3 is an impressive result, given that the GFTRI model was not obtained by optimizing the fit to the waveforms.

Figure 4 shows a similar comparison of tsunami waveforms, but for observed waveforms that were not used in the refocusing of the GFTRI source. Some of the waveform details, such as the maximum amplitude in the observed waveforms at BOSO2 and BOSO3, are not reproduced well. However, many important features, such as the dominant periods and phases are matched very well at most stations. The result also shows how well the GFTRI source based on near-field data is able to predict far-field tsunami waveforms. Observed waveforms for the 2011 Japan tsunami recorded at DART buoys 46402 and 46408 in the Aleutians and buoys 51047 and 52425 near Hawaii and Samoa, respectively, are compared with waveforms predicted using the GFTRI source and the inversion result of *Hossen et al.* [2015b]. The predicted waveforms are computed using the method of *Allgeyer and Cummins* [2014] to account for elastic loading of the seafloor and seawater density stratification as the combination of these effects is important for modeling far-field waveforms [*Watada*, 2013; *Watada et al.*, 2014; *Tsai et al.*, 2013]. The agreement between the computed waveforms and the observed data is very close, suggesting that the limited ability of the GFTRI source to resolve source kinematics makes little difference to its ability to predict far-field tsunami waveforms. We have also found excellent agreement between simulated with observed waveforms at additional DART buoys in the East, North, and Central Pacific (Figure S5).

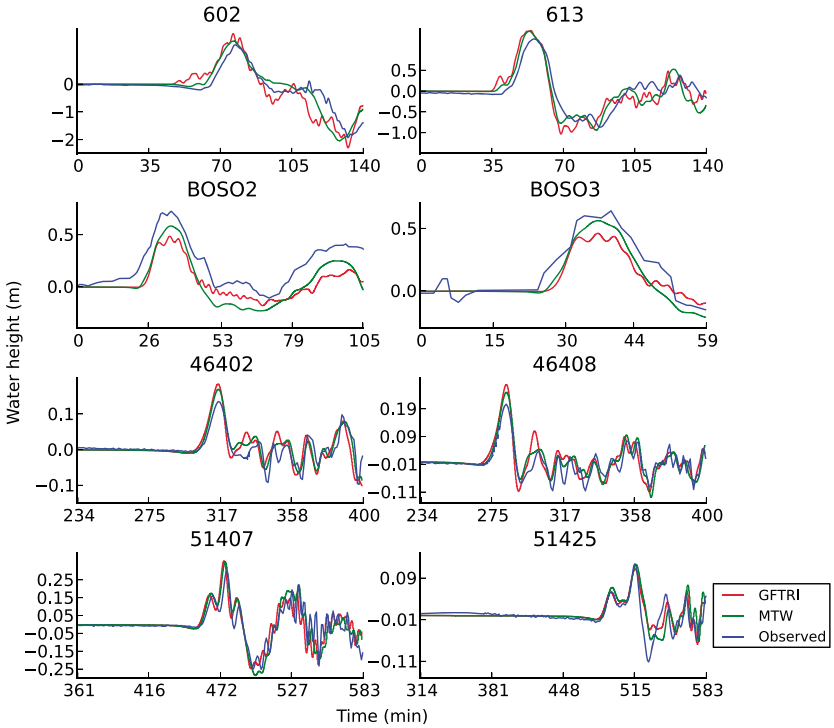

Figure 4. Comparison of observed (first and second rows) near-field and (third and fourth rows) far-field tsunami waveforms that were not used to estimate the GFTRI source in Figure 2a. Observed (blue) waveforms are compared with those calculated using the $t = 0$ source model in Figure 2a (red) and the inversion result multiple time window (MTW) of *Hossen et al.* [2015b], Figure 2b (green).

6. Discussion and Conclusion

We have developed a new approach to directly estimate the sea surface displacement that acts as a tsunami source by Green's function-based time reverse imaging of tsunami waveforms. This method estimates the tsunami source without prior assumptions regarding the excitation mechanism (i.e., it does not assume fault orientation, geometry, or slip), and without subjective weights and regularization choices that are necessary for conventional source inversion methods. The method only involves convolution of a set of Green's functions with time-reversed observed waveforms and is therefore highly computationally efficient which makes it viable for tsunami forecasting in near real time.

To demonstrate the potential of the GFTRI method for use in tsunami forecasting, we applied the source model inferred using our new method with near-field data to compute tsunami waveforms and compare them with both near-field and far-field observations that were not used in the source estimation. The near-field waveforms are recorded within 2 h of the earthquake origin time, and the source imagining produced from them is able to predict waveforms arriving at 4 h or later. The computed waveforms produce most of the first-order features of near-field waveforms such as amplitude extrema and dominant period, while the computed far-field waveforms are in excellent agreement with observed data (Figure 4). Since in an actual forecasting scenario the extent of the source area may be poorly known, in Figure S3 we have considered the effect of extending the source grid an extra 100 km to the north and south of that considered in Figure 2. Although artifacts appear in the sea surface displacement to the north and south of the actual source area, they form in shallow water depth where the apparent tsunami generation is much weaker. Furthermore, we can expect that the method requires a good azimuthal spread of observations; we have found that similar results for the 2011 Tohoku event can be obtained even if we reduce the number of waveforms used from 14 to 8 (see Figures S8 and S9). But whether the method can be used in regions like the Chilean or Tonga-Kermadec subduction zones, where far fewer observations are available, is an important question that requires further study.

There are some limitations of the proposed method. For example, the method requires good azimuthal coverage of observations to obtain high-quality parameter estimates of the source. Second, those observations

located over or near to the source grid may violate the reciprocity principle. Therefore, we only consider observations at distances greater than the tsunami wavelength from the source region. The method also uses precomputed Green's functions, which are required to be computed for the source region of interest and the particular stations and gauges to be used for the source estimation. However, it seems likely that these computations can be undertaken in real time if necessary [see, e.g., *Oishi et al.*, 2015], particularly since the computations are linear.

Acknowledgments

This work was supported by Australian Research Council Discovery Project grant DP120103207. We are grateful for many stimulating discussions about this study with Sebastien Allgeyer, Stephen Roberts, Malcolm Sambridge, and Surya Pachhai. In this study we used tsunami waveform data recorded by observation systems which are operated by the Port and Airport Research Institute (PARI), the Japan Agency for Marine-Earth Science and Technology (JAMSTEC), the Japan Meteorological Agency (JMA), the University of Tokyo's Earthquake Research Institute (ERI), and the National Oceanic and Atmospheric Administration (NOAA). This research was undertaken with the assistance of resources from the National Computational Infrastructure (NCI), which is supported by the Australian Government.

References

Allgeyer, S., and P. Cummins (2014), Numerical tsunami simulation including elastic loading and seawater density stratification, *Geophys. Res. Lett.*, *41*, 2368–2375, doi:10.1002/2014GL059348.

Ammon, C. J., T. Lay, H. Kanamori, and M. Cleveland (2011), A rupture model of the 2011 off the Pacific coast of Tohoku earthquake, *Earth Planets Space*, *63*(7), 693–696, doi:10.5047/eps.2011.05.015.

Baba, T., N. Takahashi, Y. Kaneda, Y. Inazawa, and M. Kikkojin (2014), Tsunami inundation modeling of the 2011 Tohoku earthquake using three-dimensional building data for Sendai, Miyagi Prefecture, Japan, in *Tsunami Events and Lessons Learned, Advances in Natural and Technological Hazards Research*, vol. 35, edited by T. Baba et al., pp. 89–98, Springer, Netherlands, doi:10.1007/978-94-007-7269-4_3.

Bazargani, F., and R. Snieder (2013), Optimal wave focusing for imaging and microseismic event location, chap. 890, pp. 4595–4600, SEG Technical Program Expanded, Colo., doi:10.1190/segam2013-0423.1.

Borrero, J., R. Bell, C. Csato, W. DeLange, D. Greer, D. Goring, V. Pickett, and W. Power (2013), Observations, effects and real time assessment of the March 11, 2011 Tohoku-oki Tsunami in New Zealand, *Pure Appl. Geophys.*, *170*, 1229–1248, doi:10.1007/s00024-012-0492-6.

Cummins, P. R., S. Hirano, and Y. Kaneda (1998), Refined coseismic displacement modeling for the 1994 Shikotan and Sanriku-oki earthquakes, *Geophys. Res. Lett.*, *25*(17), 3219–3222.

Gica, E., M. C. Spillane, V. V. Titov, C. D. Chamberlin, and J. C. Newman, (2008), Development of the forecast propagation database for NOAA's Short-term Inundation Forecast for Tsunamis (SIFT), Tech. Memo. OAR PMEL-139, NOAA Pac. Mar. Environ. Lab., Seattle, Wash.

Greenslade, D., et al. (2014), An assessment of the diversity in scenario-based tsunami forecasts for the Indian Ocean, *Cont. Shelf Res.*, *79*, 36–45.

Hirata, K., et al. (2002), Real-time geophysical measurements on the deep seafloor using submarine cable in the southern Kurile subduction zone, *IEEE J. Oceanic Eng.*, *27*(2), 170–181, doi:10.1109/JOE.2002.1002471.

Hossen, M. J., P. R. Cummins, S. G. Roberts, and S. Allgeyer (2015a), Time reversal imaging of the tsunami source, *Pure Appl. Geophys.*, 1–16, doi:10.1007/s00024-014-1014-5.

Hossen, M. J., P. R. Cummins, J. Dettmer, and T. Baba (2015b), Tsunami waveform inversion for sea surface displacement following the 2011 Tohoku earthquake: Importance of dispersion and source kinematics, *J. Geophys. Res. Solid Earth*, *120*, 6452–6473, doi:10.1002/2015JB011942.

Inderfurth, K., D. Fabrycky, and S. Cohen (2005), *The 2004 Indian Ocean Tsunami: Six Month Report*, The Sigur Center Asia Papers 23, Washington, D. C.

Jamelot, A., and D. Reymond (2015), New tsunami forecast tools for the French Polynesia tsunami warning system. Part II: Numerical modelling and tsunami height estimation, *Pure Appl. Geophys.*, *172*(3–4), 805–819, doi:10.1007/s00024-014-0997-2.

Kawakatsu, H., and J.-P. Montagner (2008), Time-reversal seismic-source imaging and moment-tensor inversion, *Geophys. J. Int.*, *175*(2), 686–688, doi:10.1111/j.1365-246X.2008.03926.x.

Korolev, Y. P. (2011), An approximate method of short-term tsunami forecast and the hindcasting of some recent events, *Nat. Hazards Earth Syst. Sci*, *11*, 3081–3091.

Kowalik, Z., W. Knight, and T. Logan (2005), Numerical modeling of the global tsunami: Indonesian tsunami of 26 December 2004, *Sci. Tsunami Hazards*, *23*(1), 40–46.

Larmat, C., J.-P. Montagner, M. Fink, Y. Capdeville, A. Tourin, and E. Clévédé (2006), Time-reversal imaging of seismic sources and application to the great Sumatra earthquake, *Geophys. Res. Lett.*, *33*, L19312, doi:10.1029/2006GL026336.

Larmat, C., J. Tromp, Q. Liu, and J.-P. Montagner (2008), Time reversal location of glacial earthquakes, *J. Geophys. Res.*, *113*, B09314, doi:10.1029/2008JB005607.

Maeda, T., K. Obara, M. Shinohara, T. Kanazawa, and K. Uehira (2015), Successive estimation of a tsunami wavefield without earthquake source data: A data assimilation approach toward real-time tsunami forecasting, *Geophys. Res. Lett.*, *42*, 7923–7932, doi:10.1002/2015GL065588.

National Geophysical Data Center/World Data Service (2015), Global historical tsunami database, Natl. Geophys. Data Cent., NOAA, doi:10.7289/V5PN93H7. [Available at http://www.ngdc.noaa.gov/nndc/struts/form?t=101650&s=70&d=7.]

Oishi, Y., F. Imamura, and D. Sugawara (2015), Near-field tsunami inundation forecast using the parallel TUNAMI-N2 model: Application to the 2011 Tohoku-Oki earthquake combined with source inversions, *Geophys. Res. Lett.*, *42*, 1083–1091, doi:10.1002/2014GL062577.

Percival, D. B., D. W. Denbo, M. C. Eble, E. Gica, H. O. Mofjeld, M. C. Spillane, L. Tang, and V. V. Titov (2011), Extraction of tsunami source coefficients via inversion of DART buoy data, *Nat. Hazards*, *58*(1), 567–590.

Saito, T., and T. Furumura (2009), Three-dimensional simulation of tsunami generation and propagation: Application to intraplate events, *J. Geophys. Res.*, *114*, B02307, doi:10.1029/2007JB005523.

Saito, T., Y. Ito, D. Inazu, and R. Hino (2011), Tsunami source of the 2011 Tohoku-Oki earthquake, Japan: Inversion analysis based on dispersive tsunami simulations, *Geophys. Res. Lett.*, *38*, L00G19, doi:10.1029/2011GL049089.

Satake, K., Y. Fujii, T. Harada, and Y. Namegaya (2013), Time and space distribution of coseismic slip of the 2011 Tohoku earthquake as inferred from tsunami waveform data, *Bull. Seismol. Soc. Am.*, *103*(2B), 1473–1492, doi:10.1785/0120120122.

Tang, L., et al. (2012), Direct energy estimation of the 2011 Japan tsunami using deep-ocean pressure measurements, *J. Geophys. Res.*, *117*, 2156–2202, doi:10.1029/2011JC007635.

Tappin, D. R., P. Watts, and S. T. Grilli (2008), The Papua New Guinea tsunami of 17 July 1998: Anatomy of a catastrophic event, *Nat. Hazards Earth Syst. Sci.*, *8*(2), 243–266.

Tappin, D. R., S. T. Grilli, J. C. Harris, R. J. Geller, T. Masterlark, J. T. Kirby, F. Shi, G. Ma, K. K. S. Thingbaijam, and P. M. Mai (2014), Did a submarine landslide contribute to the 2011 Tohoku tsunami?, *Mar. Geol.*, *357*, 344–361.

Titov, V. V., F. I. Gonzalez, E. N. Bernard, M. C. Eble, H. O. Mofjeld, J. C. Newman, and A. J. Venturato (2005), Real-time tsunami forecasting: Challenges and solutions, *Nat. Hazards*, *35*, 35–41, doi:10.1007/s11069-004-2403-3.

Tsai, V. C., J. P. Ampuero, H. Kanamori, and D. J. Stevenson (2013), Estimating the effect of Earth elasticity and variable water density on tsunami speeds, *Geophys. Res. Lett.*, *40*, 492–496, doi:10.1002/grl.50147.

Tsushima, H., R. Hino, H. Fujimoto, Y. Tanioka, and F. Imamura (2009), Near-field tsunami forecasting from cabled ocean bottom pressure data, *J. Geophys. Res.*, *114*, B06309, doi:10.1029/2008JB005988.

Wang, D., et al. (2012), Real-time forecasting of the April 11, 2012 Sumatra tsunami, *Geophys. Res. Lett.*, *39*, L19601, doi:10.1029/2012GL053081.

Watada, S. (2013), Tsunami speed variations in density-stratified compressible global oceans, *Geophys. Res. Lett.*, *40*, 4001–4006, doi:10.1002/grl.50785.

Watada, S., S. Kusumoto, and K. Satake (2014), Traveltime delay and initial phase reversal of distant tsunamis coupled with the self-gravitating elastic Earth, *J. Geophys. Res. Solid Earth*, *119*, 4287–4310, doi:10.1002/2013JB010841.

Wei, Y., C. Chamberlin, V. Titov, L. Tang, and E. Bernard (2013), Modeling of the 2011 Japan tsunami: Lessons for near-field forecast, *Pure Appl. Geophys.*, *170*(6–8), 1309–1331, doi:10.1007/s00024-012-0519-z.

Wells, D. L., and K. J. Coppersmith (1994), New empirical relationships among magnitude, rupture length, rupture width, rupture area, and surface displacement, *Bull. Seismol. Soc. Am.*, *84*, 974–1002.

Wilson, R. I., A. R. Admire, J. C. Borrero, L. A. Dengler, M. R. Legg, P. Lynett, and P. M. Whitmore (2013), Observations and impacts from the 2010 Chilean and 2011 Japanese tsunamis in California (USA), *Pure Appl. Geophys.*, *170*(6–8), 1127–1147.

Yue, H., and T. Lay (2011), Inversion of high-rate (1 sps) GPS data for rupture process of the 11 March 2011 Tohoku earthquake (M_w 9.1), *Geophys. Res. Lett.*, *38*, L00G09, doi:10.1029/2011GL048700.